



Clickable amino acid derivative tuned self-assembly of antigen and adjuvant for cancer immunotherapy

Xiao He^a, Lan Yang^a, Hang Su^a, Shan Lin^a, Dongmei Qi^a, Hui Chen^{a,*}, Yunfei Qu^{b,*}, Libing Liu^{c,*}, Xuli Feng^{a,*}

^a Chongqing Key Laboratory of Natural Product Synthesis and Drug Research, School of Pharmaceutical Sciences, Chongqing University, Chongqing 401331, China

^b Department of Cardiovascular Surgery, Chongqing University Three Gorges Hospital, Chongqing 404000, China

^c Institute of Chemistry, Chinese Academy of Sciences, Beijing 100190, China

ARTICLE INFO

Keywords:

Clickable amino acid
Antigen self-assembly
Copper free click reaction
Combinatorial screening
Immunotherapy

ABSTRACT

Amino acid-tuned self-assembly has become an attractive strategy for constructing various functional materials. Here, a series of dibenzocyclooctyne (DIBO) functionalized amphiphilic amino acid derivatives are designed and screened as building blocks of functional supramolecular self-assembly nanoparticles for cancer immunotherapy. One top-performing supramolecular self-assembly material (named DA6C1) is identified through combinatorial screening, and spherical nanoparticles can be easily prepared by this material tuned multicomponent synergistic self-assembly of ovalbumin (OVA) and CpG oligonucleotide. DA6C1 based nanovaccine can significantly enhance the cellular uptake of OVA and CpG into the same bone marrow derived dendritic cells (BMDCs) and greatly improve the activation of DCs. Moreover, after subcutaneous injection, this nanovaccine flows rapidly to the lymph nodes and elicits strong immune responses to achieve effective prophylactic and therapeutic effect. Therefore, our work highlights the great potential of clickable amino acid derivatives as a convenient and powerful tool to construct nanovaccine for effective immunotherapy.

1. Introduction

Cancer immunotherapy can recognize and attack cancer cells by activating or enhancing the innate immune system [1,2]. In the past few years, a variety of encouraging cancer immunotherapies, including immune checkpoint blockade therapy, chimeric antigen receptor T cell therapy and cancer vaccines, have been developed and shown promising therapeutic responses in the clinic [3–6]. Among these immunotherapies, cancer vaccines that can elicit long-lasting tumor specific immune responses have attracted great attention [7–9]. Compared with traditional live-attenuated or inactivated vaccines, subunit vaccines based on protein/peptide antigen have been extensively investigated owing to their relatively low costs and improved safety [10–13]. However, protein or peptide antigen is easy to be degraded and quickly cleared in vivo, which can only induce weak and transient immune response [14]. One promising strategy to address these problems is to develop a vaccine based on nanoparticles [15–20]. Up to now, various carriers, including gold nanoparticles, liposomes, mesoporous silica nanoparticles, poly (lactic-co-glycolic acid) nanoparticles, polymer nanoparticles and DNA

materials, have been explored to co-deliver antigen and adjuvant into APCs [21–26]. Although significant progress has been made, these methods also have their shortcomings, such as tedious and lengthy synthetic procedures, cumbersome preparation process of these formulations and the requirement of modification of antigen, which inevitably would result in low efficiency in eliciting antigen-specific immunogenicity [27–29]. Therefore, there is a growing demand for more easily manufactured vectors, which can not only deliver intact antigen and adjuvant to the same APC, but also raise strong immune responses.

Self-assembly plays a vital role in regulating the functionalities of many biological systems [30–35]. Proteins, peptides, and even amino acids have been employed as building blocks to construct various self-assembled supramolecular nanomaterials for a wide range of potential applications [36–41]. Hydrogels formed by peptide self-assembly have been applied for immunomodulation, inducing antigen specific humoral immunity and cellular immune response [42]. In addition, compared with peptides, amino acids and their derivatives (e.g., fluorenylmethoxycarbonyl (Fmoc) modified amino acids) have simple structure, good biocompatibility, repeatability and operability [43],

* Corresponding authors.

E-mail addresses: chenhui0429@cqu.edu.cn (H. Chen), quyunfei200@163.com (Y. Qu), liulibing@iccas.ac.cn (L. Liu), fengxuli@cqu.edu.cn (X. Feng).

<https://doi.org/10.1016/j.jconrel.2021.07.033>

Received 19 February 2021; Received in revised form 25 June 2021; Accepted 21 July 2021

Available online 24 July 2021

0168-3659/© 2021 Elsevier B.V. All rights reserved.

thus, they have greater attraction and potential in the self-assembly of functional supramolecular nanocarriers for drug delivery. However, there are few reports on these self-assembled nanomaterials for efficient protein antigen encapsulation and delivery. Therefore, it is necessary to prepare and expand new amino acid derivatives to construct functional self-assembled nanoparticles to achieve efficient delivery of protein antigen and oligonucleotide adjuvant for immunotherapy.

Herein, we investigated the ability of a combinatorial library of DIBO protected amphiphilic arginine derivatives (DA1–6) and multi-claw azide functionalized small molecule crosslinkers (C1–3) (their synthetic routes were shown in Fig. 1A and B) as building blocks for functional supramolecular self-assembled nanovectors to enable intracellular delivery of protein antigen and oligonucleotide adjuvant. The negatively charged OVA and CpG can be easily incorporated into the structure of amphiphilic arginine derivatives by simply mixing them together at room temperature, and the architecture of this self-assembled nanocomposite can be further strengthened by the introduction of cross-linking agent (Fig. 1C). The nanovaccine constructed with this self-assembly scheme showed enhanced DC uptake and much more antigen cross-presentation to trigger DC maturation. After subcutaneous injection, such nanovaccine could effectively migrate to lymph nodes and elicit strong immune responses to achieve effective prophylactic and therapeutic effect. Therefore, our work highlights the great potential of the self-assembled clickable amino acid derivatives as an attractive and powerful tool for the development of nanovaccines for cancer immunotherapy.

2. Results

2.1. Preparation and screening of high efficiency protein transporter

We first investigated and screened effective antigen delivery carriers by the combination assembly of different amino acid derivatives DA1–6 and multi-claw cross-linking agents C1–3. As shown in Fig. 2A, self-assembled nanoparticles can easily be formed after dissolving amphiphilic arginine derivatives DA1–6 into aqueous solution. Antigen OVA can be incorporated into the structure of self-assembled nanoparticles based on hydrophobic and electrostatic interactions. And the architecture of self-assembled nanoparticles can be further strengthened by the introduction of cross-linking agents C1–3. The agarose gel retention assay in Fig. 2B indicated that amphiphilic arginine derivatives with longer alkyl chain, such as DA5 and DA6, had good OVA encapsulation ability. In addition, the introduction of cross-linking agents further enhanced their protein entrapment efficiency, and cross-linker C1 and C3 showed better improvement in protein encapsulation capability than that of cross-linker C2. Next, the intracellular OVA delivery efficiency of various self-assembled nanoparticles was evaluated by co-culturing RAW 264.7 cells with FITC-OVA loaded nanocomposites. Quantitative flow cytometry analysis in Fig. 2C showed that most FITC-OVA loaded nanocomposites could pass through the cell membrane and effectively transport the encapsulated OVA into the cytoplasm. Among them, the nanoformulation based on the combination of C1 with DA6 (DA6C1) exhibited the best endocytosis effect, and it also showed efficient encapsulation of other proteins, such as bovine serum albumin (BSA) (Fig. S1). Therefore, these data indicated that self-assembled

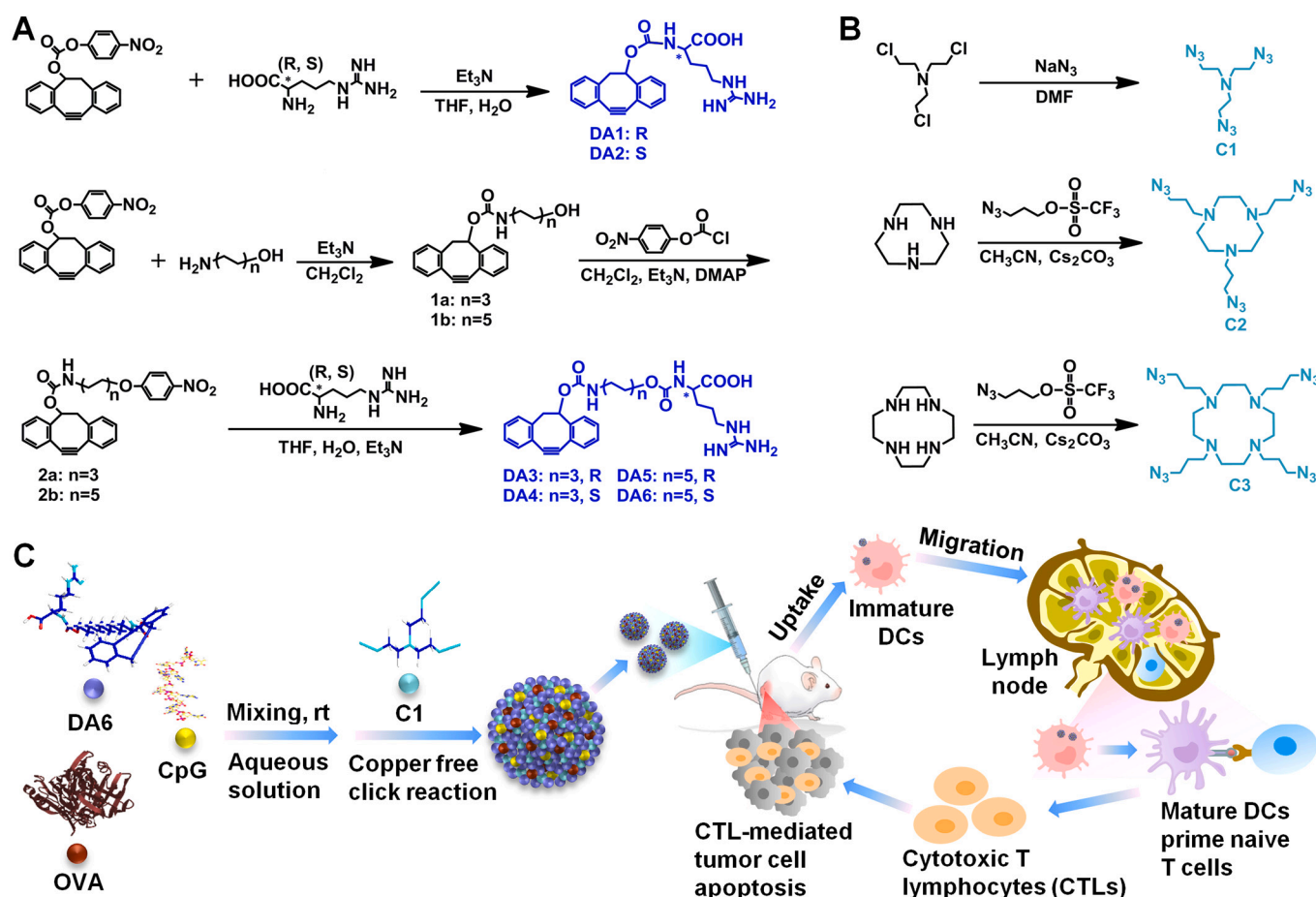


Fig. 1. DBCO functionalized amphiphilic amino acid derivatives were designed for constructing functional materials for effective cancer immunotherapy. (A) Synthetic routes of DBCO functionalized amphiphilic amino acid derivatives DA1–6 and (B) the multi-claw cross-linking agents C1–3. (C) Schematic illustration of representative self-assembled nanovaccine for effective cancer immunotherapy.

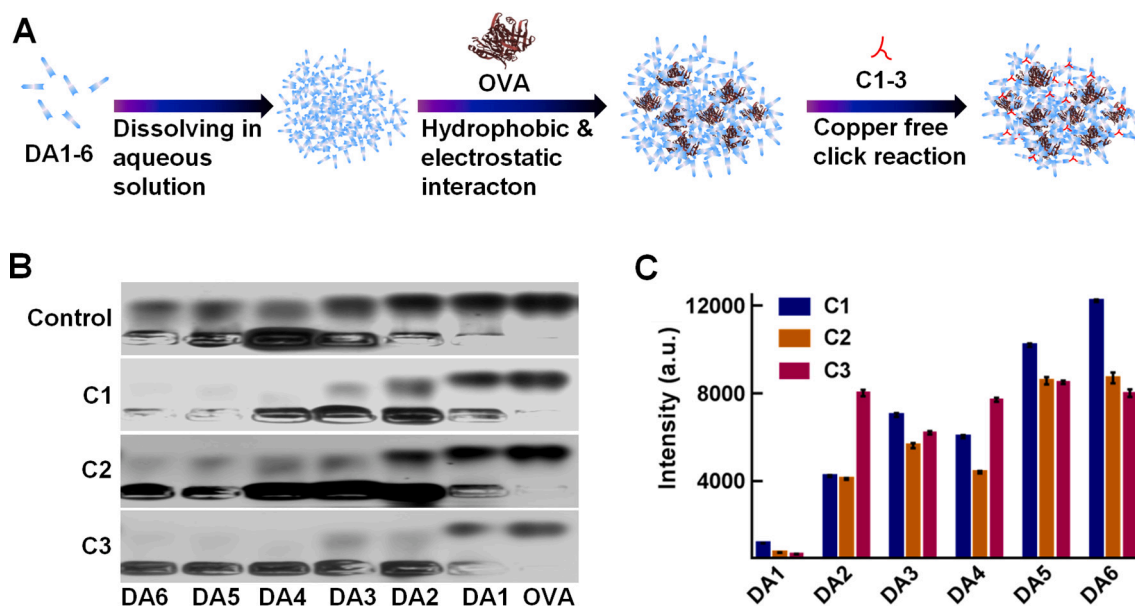


Fig. 2. Combination screening of effective protein antigen carriers. (A) Schematic diagram of the formation of self-assembled protein antigen nanoparticles. (B) Agarose gel retention assay for evaluating the protein encapsulation efficiency of different combinations of self-assembled nanoparticles. (C) Flow cytometry quantitative analysis of intracellular FITC-OVA delivery efficacies of various self-assembled nanoformulations.

nanoparticles based on DA6C1 appeared to be the most potential protein antigen nanocarrier for immunotherapy.

2.2. Characterization of different nanoformulations

Further studies were employed to elucidate the nanostructures of various nanoformulations based on the self-assembly of DA6. As shown in Fig. 3A, amphiphilic DA6 itself was prone to self-assemble into nanoparticles based on π - π stacking interaction, and spherical nanoparticles were observed by transmission electron microscopy (TEM). Dynamic light-scattering (DLS) experiments revealed that the average diameter of DA6 nanoparticles was approximately 100 nm (Fig. 3B). The addition of crosslinker C1 into the aqueous solution of DA6 had no effect on its spherical morphology, but just increased the size due to the less compact arrangement. Similarly, further encapsulation of OVA and CpG only increased the particle size and greatly reduced the zeta potential of DA6C1/OVA (Fig. 3C). To gain insight into the molecular configuration and arrangement of the self-assembled nanostructures, UV-vis absorption, fluorescence and circular dichroism (CD) spectrum were applied to

investigate the intermolecular interactions within various nanoformulations. As shown in Fig. 3D, DA6 has strong absorption in the wavelength range of 280 nm to 310 nm. However, after the introduction of C1, the absorption disappeared and the fluorescence was enhanced (Fig. 3E), which indicated that the effective chemical crosslinking occurred via copper free click reaction. In addition, neither the encapsulation of OVA nor the further binding with CpG caused further changes in the absorption or fluorescence of DA6C1, implying that the nanocomposites were formed mainly through coordination driven self-assembly. Moreover, the CD spectra shown in Fig. 3F revealed that DA6 was in a random unstructured aggregation state in aqueous solution. The addition of cross-linking agent C1 only caused the red shift of the CD signal around 195–200 nm, but did not change the conformation. Similarly, encapsulation of antigen OVA with DA6C1 nanoparticles did not induce the conformation change of antigen protein OVA. These results collectively implied that self-assembled nanoparticles based on DA6C1 could be employed as carriers for protein antigen and oligonucleotide adjuvant delivery.

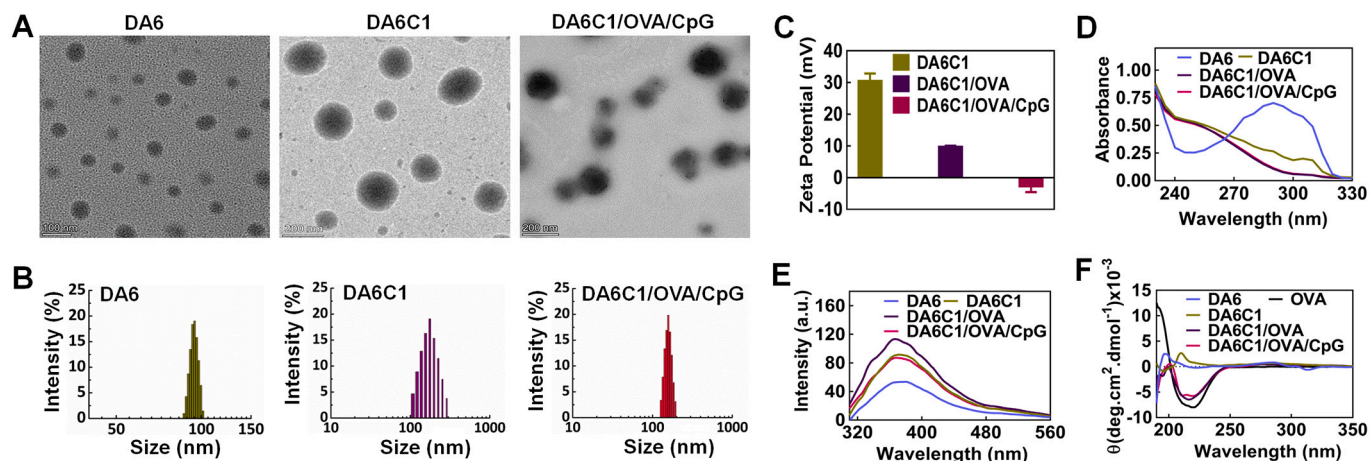


Fig. 3. Characterization of nanoformulations based on self-assembly of DA6C1. (A) TEM images, (B) size distribution and (C) zeta potentials of various complexes based on DA6C1. (D) UV-visible absorption, (E) fluorescence and (F) CD spectra of various self-assembled nanoparticles based on DA6C1.

2.3. Cell uptake and in vitro immune activation

Nanovaccines must be endocytosed into the cytoplasm to achieve the specific immune response and protective effect, therefore, the cell uptake of nanovaccines based on DA6C1 was evaluated. Fig. 4A showed the confocal fluorescence images of BMDCs after incubation with the combination of FITC labeled OVA (OVA-FITC) and rhodamine labeled CpG (CpG-ROD) or DA6C1 based nanovaccines co-loaded with OVA-FITC and CpG-ROD. Negligible fluorescence was observed in free OVA+CpG group, in contrast, strong fluorescence of OVA-FITC and CpG-ROD was observed in DA6C1 nanovaccine group, indicating that DA6C1 based nanovaccine could significantly enhance the cellular uptake of OVA and CpG. Such a phenomenon was further confirmed by

flow cytometric analysis (Fig. 4B). In addition, the co-localization of green/red fluorescence signals validated that both the antigen OVA and adjuvant CpG were internalized into the same DCs.

Next, the effect of DA6C1 based nanovaccine on the antigen cross-presentation and the maturation of DCs was further investigated. Flow cytometry analysis was employed to analyze the percentage of SIINFEKL⁺ DCs and CD86⁺CD80⁺ DCs to evaluate the efficiency of antigen cross-presentation and DC maturation. The results showed that DA6C1 based nanovaccine significantly increased the levels of antigen cross-presentation (Fig. 4C, E) and DC maturation (Fig. 4D, F), while no appreciable DC stimulation effect was observed in cells treated with free OVA+CpG. In addition, compared with the nanovaccines only encapsulated with antigen, the nanovaccines obtained after adding CpG

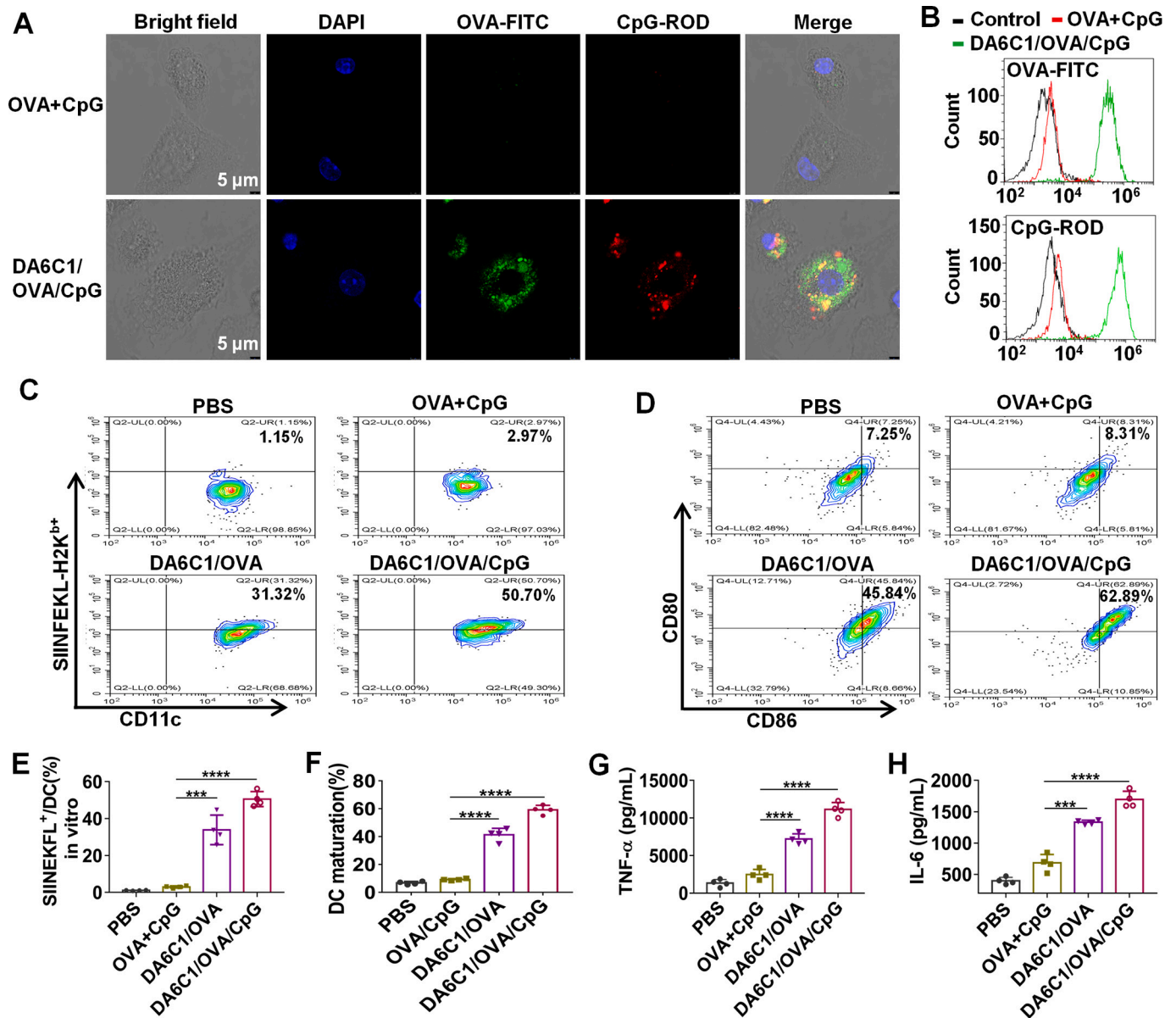


Fig. 4. In vitro BMDC uptake and activation by nanovaccines based on DA6C1. (A) Confocal fluorescence images of BMDCs after incubation with the combination of free OVA-FITC and CpG-ROD or DA6C1 nanovaccine co loaded with OVA-FITC and CpG-ROD for 20 h. Nucleus were stained with DAPI (blue channel). Scale bar = 5 μm. (B) FACS analysis of BMDCs incubated with OVA-FITC and CpG-ROD loaded DA6C1 nanovaccines to compare the cellular uptake efficiency of OVA antigen and CpG adjuvant. (C, D) Representative flow cytometry data and (E, F) the statistical data to show OVA antigen cross-presentation efficiencies and DC maturation induced by free OVA+CpG or different nanovaccine formulations in vitro. Cells were stained with antibodies against CD11c as the DC marker as well as CD80 and CD86 as DC maturation markers (gated from CD11c). (G) Secretion of TNF-α and (h) IL-6 from BMDCs after treated with free OVA+CpG or different nanovaccinations (**p < 0.01; ***p < 0.001; ****p < 0.0001). (For interpretation of the references to color in this figure legend, the reader is referred to the web version of this article.)

showed more significant antigen cross-presentation and DC maturation effect, suggesting that the simultaneous delivery of antigen and adjuvant to the same APCs was critical to enhance cellular immunity. Moreover, the secretion of immunostimulatory cytokines was recorded by the enzyme-linked immunosorbent assay (ELISA). As shown in Fig. 4G and H, the highest production of tumor necrosis factor alpha (TNF- α) and interleukin 6 (IL-6) was also found from DCs after treatment with OVA and CpG co-loaded DA6C1 based nanovaccine, which was consistent with the mature data of DC. Besides, no apparent cellular toxicity of DA6C1 could be observed, indicating that the good biocompatibility of the nanovector (Fig. S2).

2.4. In vivo tracking of labeled nanovaccine

To evaluate the ability of nanovaccines to migrate to draining lymph nodes, mice were subcutaneously injected with the combination of free rhodamine labeled OVA (OVA-ROD) and CpG, OVA-ROD or CpG co-loaded DA6C1 nanovaccine in the tail base, and then the migration efficacy of the different formulations was monitored at 1, 8, 16, 24 h post injection using in vivo fluorescence imaging (Fig. 5A, B). Compared with free OVA+CpG, DA6C1 based nanovaccines were more efficiently accumulated in the draining inguinal lymph nodes. In addition, ex vivo fluorescence imaging of major organs and lymph nodes taken at 24 h post-injection further confirmed that the DA6C1 based nanovaccine can specifically migrate to lymph nodes (Fig. 5C). Moreover, the fluorescent signal at the site of administration was also monitored by in vivo imaging system. As shown in Fig. 5D and E, the fluorescence of free OVA+CpG decreased rapidly and no fluorescence can be detected 5 days post-injection. In contrast, the nanovaccines based on DA6C1 were cleared gradually, and fluorescence could still be detected 15 days after injection, indicating that our self-assembled nanoparticles can effectively protect antigens and enhance their retention rate.

2.5. In vivo immunostimulatory activities

We have assessed the effects of different antigen formulations on DC maturation in vitro, and then we continued to evaluate the abilities of these vaccines to improve DC maturation in vivo. Mice were subcutaneously immunized with PBS, OVA+CpG, DA6C1/OVA or DA6C1/OVA/CpG with equal amount of OVA (2.5 mg/kg) and CpG (100 μ g/kg),

respectively. To explore the effect of various antigen and adjuvant formulations on the immunological responses, mice were sacrificed on day 7 post final immunization to collect their inguinal draining lymph nodes to evaluate the efficiency of antigen cross-presentation and DC maturation (Fig. S3). The percentages of SIINFEKL⁺ DCs and CD86⁺CD80⁺ matured DCs were greatly increased in DA6C1 based nanovaccines compared with PBS and free OVA+CpG groups (Fig. 6A, B). Moreover, the highest levels of immunostimulatory cytokines including TNF- α , IFN- γ and IL-6 were also found in the serum of mice treated with DA6C1/OVA/CpG (Fig. 6C-E). These results indicated that the DA6C1 based nanovaccines could more efficiently elicit in vivo immune responses than other groups.

The immunostimulatory effects of various antigen formulations on antigenic specific humoral immune response were evaluated. Compared with free OVA+CpG, DA6C1/OVA/CpG significantly increased OVA-specific IgG titers (Fig. 6F), which could be due to the reason that DA6C1 nanocarriers facilitated the effective migration of nanovaccines to the lymph nodes and enabled the co-delivery of OVA and CpG into the same APCs, thus generating much high immune responses. Moreover, the activation of antigen-specific CD8⁺ and CD4⁺ T cells, which are critical to induce cellular and humoral immune response, was also evaluated. After three times of inoculation, the splenocytes were harvested and stimulated with OVA (50 μ g/mL), and the cells were stained with antibodies of FITC-anti-CD3 and APC-anti-CD4 or PE-anti-CD8 for FACS analysis (Fig. S4). As shown in Fig. 6G and H, DA6C1/OVA/CpG treatment exhibited the highest induction of CD4⁺ T cells and CD8⁺ T cells proliferation compared with PBS, OVA+CpG. In order to further evaluate the cytotoxicity of endogenous T cell response, the production of IFN- γ in re-stimulated splenocytes was detected by ELISA. Fig. 6I showed that the levels of IFN- γ were significantly increased in DA6C1/OVA/CpG group compared with other groups. These results indicated that the nanovaccines based on DA6C1 can effectively induce humoral and cellular immunity and promote the differentiation of T cells into CTLs. Furthermore, the most important role of vaccination (Vac.) is that the body's immune system can respond quickly and effectively when exposed to the same pathogen. Hence, CCK-8 assay was performed to evaluate the effect of different antigen formulations on splenocyte proliferation responses. As shown in Fig. 6J, under the re-stimulation of OVA, the highest proliferation was observed in splenocytes collected from mice immunized with DA6C1/OVA/CpG, which could promote the

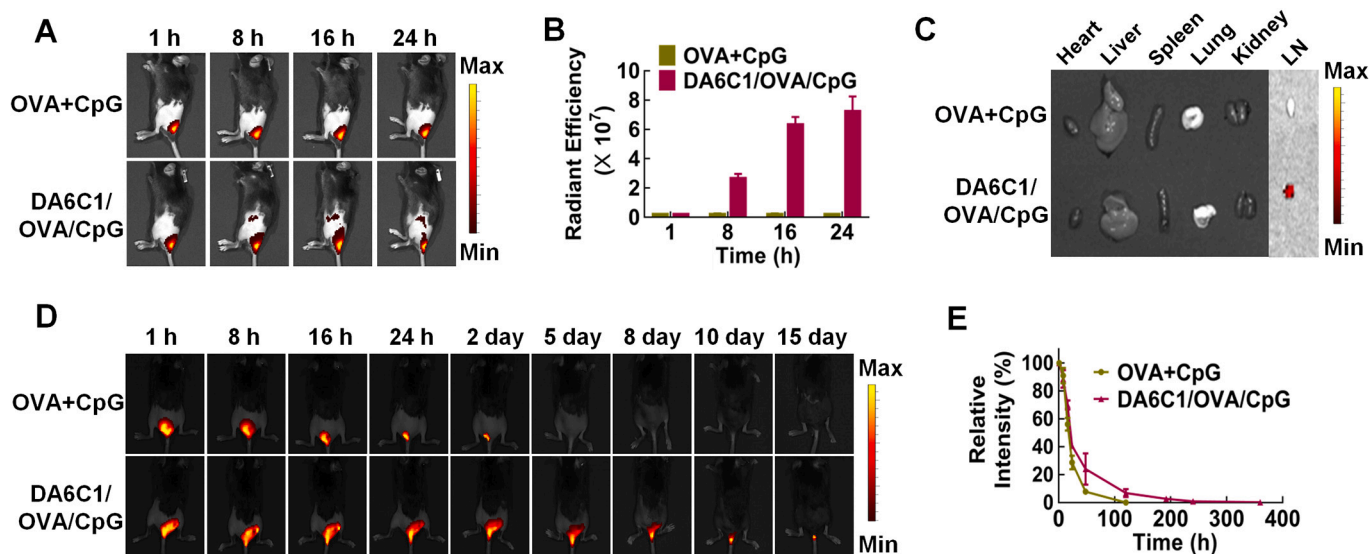


Fig. 5. In vivo tracking of DA6C1 based nanovaccines. OVA-ROD and CpG was formulated with DA6C1 nanocarrier and subcutaneously injected into C57BL/6 mice on their tail base. (A) In vivo fluorescence images and (B) quantified fluorescence signals in the draining inguinal lymph nodes at different time points after subcutaneously injection of free OVA+CpG or DA6C1/OVA/CpG. (C) Images of major organs (heart, liver, spleen, lung and kidney) and lymph nodes isolated after 24 h injection. (D) Representative fluorescent images and (E) quantified fluorescent intensity on the injection site at different time points after subcutaneously injection.

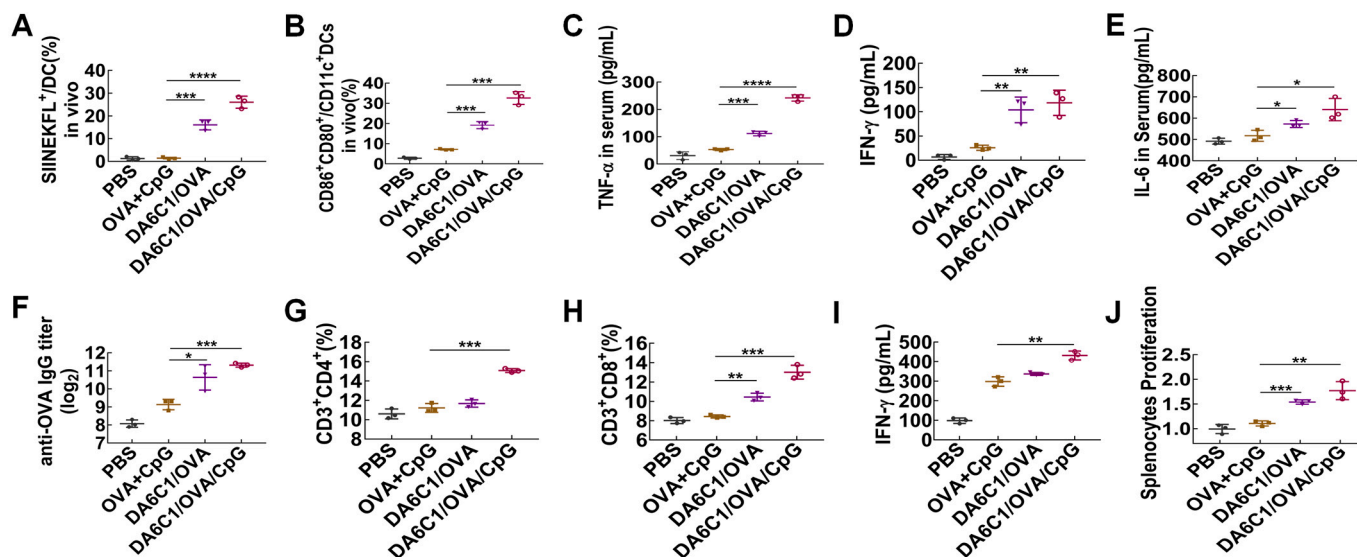


Fig. 6. Flow cytometry analysis of in vivo immune response. Statistic data to show OVA antigen cross-presentation (A) and DC maturation (B) induced by different antigen and adjuvant formulations in vivo. DCs isolated from the lymph nodes on day 7 post immunization. C-E, The production of TNF- α (C), IFN- γ (D) and IL-6 (E) from the serum of mice after immunized with Mice were immunized with PBS, OVA + CpG, DA6C1/OVA or DA6C1/OVA/CpG subcutaneously. The doses of OVA and CpG were 2.5 mg/kg and 100 μ g/kg, respectively. (F) The anti-OVA IgG secretion in mouse serum determined by ELISA. G-H, The percentages of CD4⁺ (G) and CD8⁺ T cells (H) in splenocytes purified from mice immunized by SC injection on day 0, 7 and 14. Twenty-one days later, mice were sacrificed and the isolated splenocytes were restimulated with OVA (50 μ g/mL) for 72 h at 37 °C. (I) The production of IFN- γ after splenocytes stimulated ex vivo for 72 h. (J) Splenocytes proliferation measured by CCK-8 assay. The isolated splenocytes were incubated with OVA (50 μ g/mL) for 48 h. (* p < 0.05; ** p < 0.01; *** p < 0.001; **** p < 0.0001).

strong immune response and was promising in prevention and immunotherapy.

2.6. Prophylactic effect of nanovaccines

To investigate the in vivo tumor challenge, we evaluated the prophylactic effects of various vaccine formulations by using an E.G7-OVA tumor model. As illustrated in Fig. 7A, mice were vaccinated with different formulations including OVA+CpG, DA6C1/OVA or DA6C1/OVA/CpG for three times at 1 week intervals. PBS was used as negative control. Seven days post the final vaccination, 5×10^5 E.G7-OVA tumor cells were subcutaneously injected into the mice. As shown in Fig. 7B and C, DA6C1/OVA treatment exhibited delayed tumor growth

compared to untreated PBS control group and free OVA+CpG group. And the tumor progression was further retarded by vaccination with DA6C1/OVA/CpG. Furthermore, survival rate analysis (Fig. 7D) showed that mice treated by PBS and free OVA+CpG were euthanized within 23 days. In contrast, DA6C1/OVA immunization prolonged the survival time to 33 days. More importantly, the survival rate of the mice treated with DA6C1/OVA/CpG was greatly increased 60% on day 45 and 2 out of 5 mice in this treatment group became tumor-free for over 100 days. Thus, these results demonstrated that DA6C1 based nanovaccine can improve the vaccination effect.

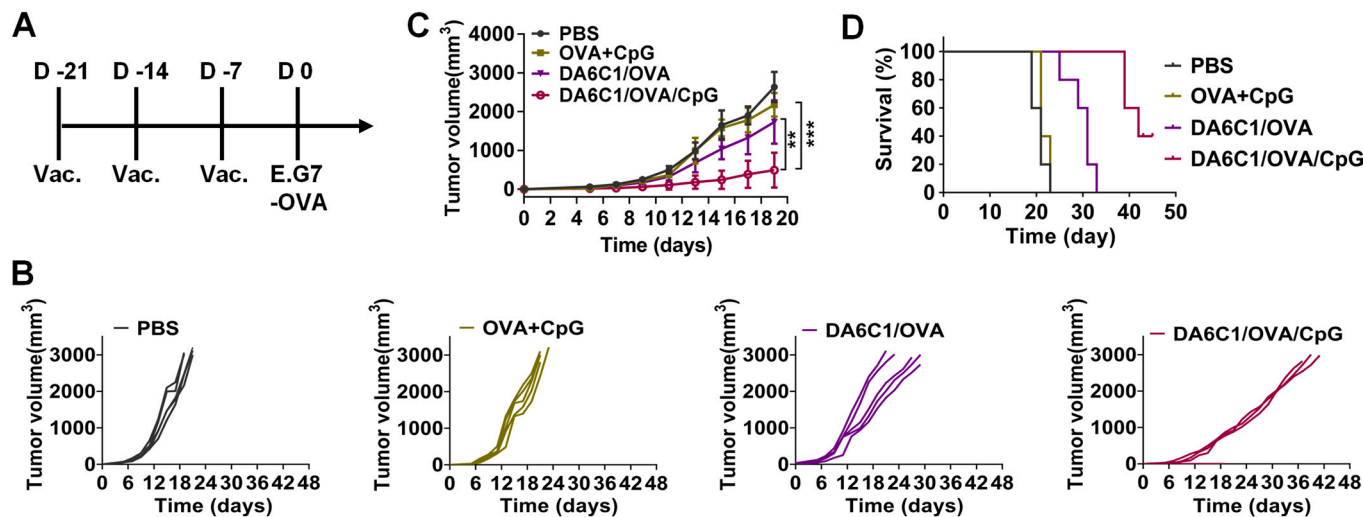


Fig. 7. Antitumor activities of various nanoformulations as prophylactic vaccines. (A) Schematic illustration of the tumor challenge experiment design. Mice were immunized three times with an interval of 1 week with different formulations. Twenty one days later, 5×10^5 E.G7-OVA tumor cells were inoculated subcutaneously. (B) Individual tumor growth curves and (C) average tumor growth curves from mice injected with tumor cells (** p < 0.01; *** p < 0.001). (D) Percentage of survival rate of mice after tumor challenge.

2.7. In vivo antitumor activity

Cancer vaccine can be combined with checkpoint blockade therapy to relieve immunosuppression and further the therapeutic effect. Therefore, we subsequently examined the therapeutic effect of DA6C1/OVA/CpG nanovaccine combined with the programmed death-1 antibody (anti-PD1) on established E.G7-OVA tumors. According to the treatment scheme shown in Fig. 8A, after inoculation of E.G7-OVA tumor cells on day 5, mice were subcutaneously immunized with various formulations for three times on days 5, 11, and 17. Anti-PD1 was intraperitoneally injected at the dose of 150 µg per mouse on day 5, 8, 11, 14 and 17 for comparison or combination therapy. PBS was used as the control group. It was shown that tumor growth was rapid in anti-PD1 group and free OVA+CpG group (Fig. 8B). While DA6C1/OVA/CpG could effectively inhibited tumor progression and improved the survival rate. Notably, DA6C1/OVA/CpG nanovaccine combined with anti-PD1 blockade immunotherapy strategy further enhanced the therapeutic effect and significantly prolonged the survival time (Fig. 8C). Histological analysis using H&E staining revealed that DA6C1/OVA/CpG/anti-PD1 exerted the strongest inhibitory effect on the progression of tumor cells (Fig. S6A). Furthermore, no damage to healthy organs such as heart, liver, spleen, lung, and kidney were observed during treatment, indicating that DA6C1 based delivery systems have good biocompatibility (Fig. S7). All these results suggested that DA6C1/OVA/CpG nanovaccine in combination with checkpoint blockade may be a promising strategy for tumor immunotherapy.

The effective infiltration of CTLs and restriction of Tregs in tumor environment play an important role in the effective treatment of tumor. To investigate the potential mechanism of the developed nanovaccines in anti-tumor progression, immunized mice were sacrificed at day 4 after the final immunization, and tumor samples were collected and analyzed by FACS and immunofluorescent staining. FACS analysis in Fig. 8D showed that compared with anti-PD1 and free OVA+CpG group, the number of CD4⁺ T and CD8⁺ T cells in tumor tissues from mice treated by DA6C1/OVA/CpG was increased (Fig. 8E, F). When combined with anti-PD1, the percentage of CD8⁺ T cells were further increased, which was confirmed by immunofluorescence staining of CD8⁺ T cells that the strongest infiltration of CD8⁺ T cells was found in the DA6C1/OVA/CpG/anti-PD1 treatment group (Fig. S6B). Meanwhile, the lowest proportion of Tregs (CD4⁺Foxp3⁺) was also demonstrated in DA6C1/OVA/CpG/anti-PD1 combination group (Fig. S5, 8G). In addition, the secretion of IFN-γ in the tumor was greatly elevated after vaccination with DA6C1/OVA/CpG nanovaccine, and the highest production of IFN-γ was observed in combination with anti-PD1 immunotherapy (Fig. 8H, S6C). Overall, these results indicated that DA6C1/OVA/CpG nanovaccine combined with anti PD-1 immunotherapy can effectively increase the infiltration of CTLs and reduce the suppression effect of Tregs cells, thus effectively inhibiting the growth of tumor.

3. Discussion

The function of maintaining intracellular homeostasis and life system

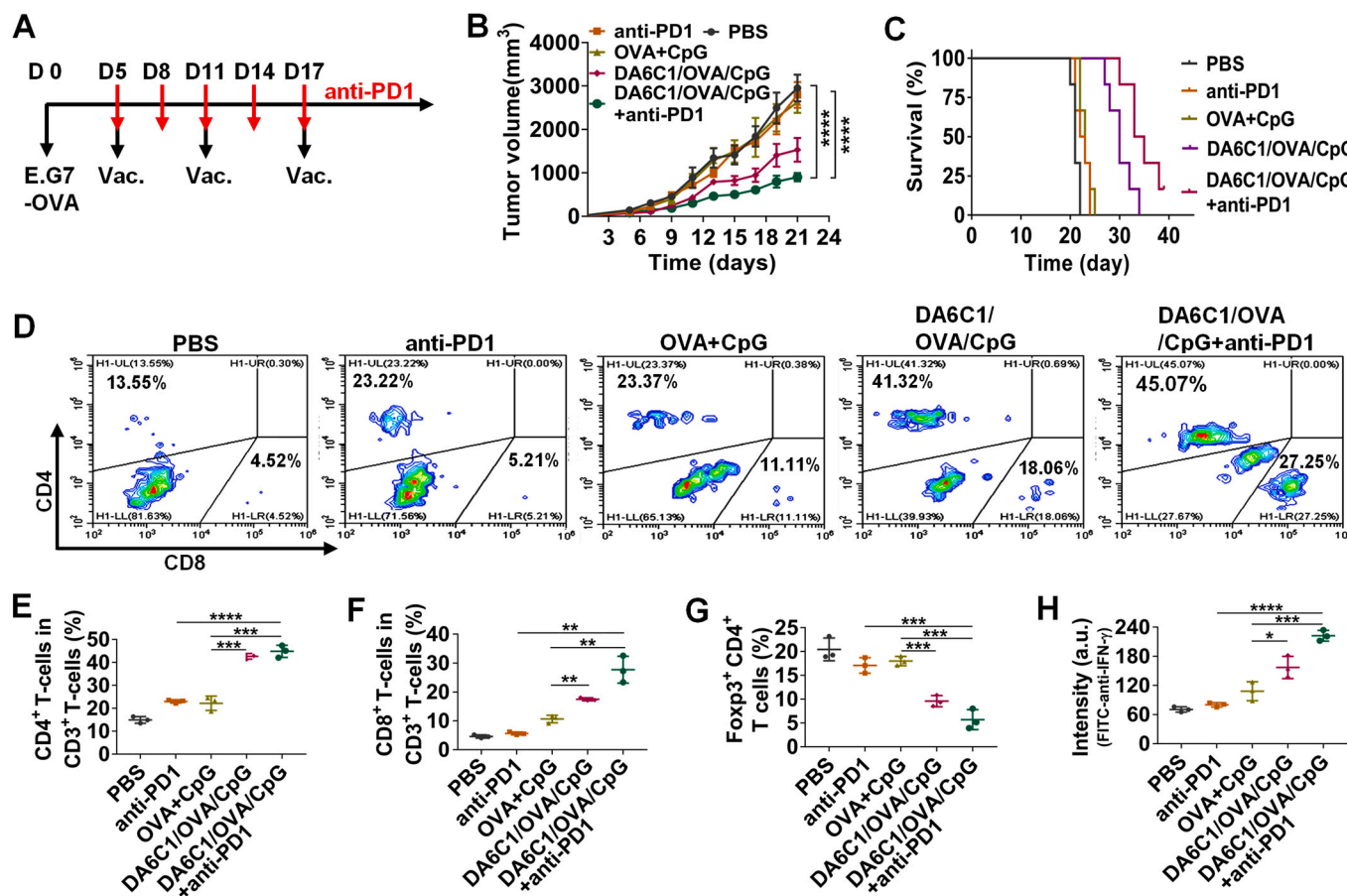


Fig. 8. Antitumor effect of different nanovaccines combined with anti-PD1 checkpoint blockade. (A) Schematic illustration showed the experimental design of nanovaccines combined with anti-PD1 therapy. Mice were inoculated subcutaneously with 5 × 10⁵ E.G7-OVA tumor cells and treated by various formulations for three times on days 5, 11, and 17. Anti-PD1 was intraperitoneally injected at the dose of 150 µg per mouse on day 5, 8, 11, 14 and 17 for comparison or combination therapy. PBS was used as the control group. (B) Average tumor growth curves and (C) percentage of survival rate of mice after various treatments. (D) Representative FACS plots of T cells in tumor tissues. The percentages of (E) CD4⁺ T cells, (F) CD8⁺ T cells, (G) regulatory T cells, and (H) the production of IFN-γ in tumors were determined by flow cytometry analysis (*p < 0.05; **p < 0.01; ***p < 0.001; ****p < 0.001).

is based on supramolecular assembly of sequence specific polymers, such as nucleic acids, proteins and peptides. Among them, peptides have attracted much attention due to their biocompatibility and chemical versatility. [37] They have been employed as building blocks to construct different supramolecular nanomaterials for a wide range of potential applications. Hydrogels formed by peptide self-assembly could apply for immunomodulation, inducing antigen specific humoral immunity and cellular immune response. [42] However, the requirement of covalent conjugation of antigen or the introduction of additional heating-cooling process hinders the further development of peptide derivatives for immunotherapy. In addition, it has been shown that the short peptide composed of two or three amino acids can be used as a powerful self-assembly motif. [43] For example, the well-known diphenylalanine peptide has been widely used to prepare various supramolecular self-assembled nanomaterials. [44,45] Nevertheless, non-aqueous solvents are not only an essential condition for the self-assembly of short peptides, but also exert a significant impact on the nanoscale morphology of short peptide self-assemblies, which seriously hinders their applications in drug delivery. At the same time, there are few reports on the supramolecular self-assembled functional nanomaterials based on single amino acid. Compared with peptides, amino acids have simpler structure, better biocompatibility, repeatability and operability, therefore, they have greater attraction and potential in the self-assembly of functional supramolecular nanocarriers for drug delivery. [46,47]. Therefore, in this study, we designed and screened a series of clickable amino acid derivatives as building blocks of functional supramolecular self-assembly nanoparticles to realize the intracellular delivery of protein antigen and oligonucleotide adjuvant into the same DCs to enhance the immune response. The traditional amino acid protecting group Fmoc was changed to DIBO functional group for copper free click chemistry, which can efficiently expand the types of self-assembled materials under mild conditions, strengthen the self-assembly behavior and avoid any non-aqueous solutions that might inactivate protein and nucleic acid. TEM and DLS experiments revealed that self-assembled nanoparticles can be easily formed with size of about 100 nm after dissolving these amphiphilic arginine derivatives into aqueous solution. Agarose gel retention assay indicated that OVA can be incorporated into the structure of self-assembled nanoparticles, and the introduction of cross-linking agents can further enhance the loading capability of these nanoparticles. Through *in vitro* combinatorial screening, we found that self-assembled nanoparticles based on DA6C1 had high antigen and adjuvant loading capacity and cellular endocytosis efficiency, indicating that nanovaccines based on DA6C1 tuned self-assembly has great potential in immunotherapy.

As an important type of APCs, DCs play a crucial role in inducing adaptive immunity by activating T cells. Nanovaccines can greatly determine the efficiency of antigen uptake and intracellular localization, thus affecting the specific immune response and protective effect. The confocal fluorescence images of BMDCs incubated with OVA and CpG co-loaded DA6C1 nanovaccines demonstrated that DA6C1 could significantly enhance the cellular uptake of OVA and CpG, and internalize them into the same DCs, which would be beneficial to induce stronger immune response and more effective immune activity. The results showed that DA6C1/OVA/CpG nanovaccine could significantly improve the efficiency of antigen cross presentation and DC activation (Fig. 4C-F), while free OVA+CpG had little effect on the stimulation of DC maturation, which was consistent with the fact that naked negative charged antigen and nucleic acid can hardly enter the cytoplasm and were also easy to be degraded by enzymes. Moreover, this nanovaccine could also produce high levels of TNF- α and IL-6 (Fig. 4G and H), which are cytokines highly related to antitumor immunity. Overall, these results suggested that the nanovaccine based on DA6C1 tuned self-assembly of OVA and CpG can greatly enhance the immune response, thus becoming an effective method for DC activation. In addition, we evaluated the abilities of these vaccines to improve DC maturation *in vivo*. DA6C1 based various nanovaccines could significantly improve

the DC maturation and antigen cross-presentation in mice by increasing the percentages of CD11c⁺ SIINFEKL⁺DCs and CD86⁺CD80⁺ matured DCs. In addition, high secretion of immunostimulatory cytokines including TNF- α , IFN- γ and IL-6 were also found in the serum of mice treated with DA6C1/OVA/CpG nanovaccine. Moreover, this nanovaccine could also increase the production of anti-OVA IgG titres in the serum of mice, enhance the activation of antigen-specific CD8⁺ and CD4⁺ T cells, and promote the proliferation of splenocytes. Therefore, the strong *in vivo* immune responses induced by DA6C1/OVA/CpG nanovaccine demonstrated its promising role in prevention and treatment of cancer.

After vaccination by using an E.G7-OVA tumor model, DA6C1/OVA/CpG nanovaccine exhibited superior to other formulations in delaying tumor development and improving survival rate. The treatment of established tumors showed that DA6C1/OVA/CpG nanovaccine significantly inhibited tumor progression and induced effective CTL infiltration. More importantly, DA6C1/OVA/CpG nanovaccine combined with anti-PD1 therapy was more effective in alleviating tumor immunosuppression, increasing the proliferation and infiltration of CTLs, thus leading to better anti-tumor treatment effect. Taken together, these results demonstrated the great potential of clickable amphiphilic amino acid derivatives tuned self-assembly of antigen and adjuvant as a convenient and powerful strategy for the development of nanovaccine to improve cancer immunotherapy.

4. Materials and methods

4.1. Materials

6-aminohexan-ol and 10-aminodecan-1-ol were purchased from 9dingchemistry (Shanghai, China). L-arginine and D-arginine was purchased from Alfa Aesar (Shanghai, China). Other chemical reagents were bought from energy chemical (Beijing, China). Ovalbumin (OVA) was obtained from Sangon Technology (Shanghai, China). CpG (5'-TCC ATG ACG TTC CTG ATG C-3') and Rhodamine-labeled CpG-ROD (5'-Rhodamine-TCC ATG ACG TTC CTG ATG-3') were synthesized by Sangon Technology (Shanghai, China). DAPI was purchased from solarbio (Beijing, China). And, TNF- α , IL-6, IFN- γ ELISA Kit was also obtained from solarbio (Beijing, China). Fluorescence labeled CD11c, CD80, CD86, SIINFEKL/H-2 kb, CD3, CD4, CD8, Foxp3 antibody, FITC-conjugated antimouse IFN- γ and HRP-conjugated antimouse IgG were obtained from Biolegend (San Diego, USA). Recombinant mouse GM-CSF and IL-4 were purchased from PeproTech (Rocky Hill, USA). RAW 264.7 cell line was bought from National Infrastructure of Cell Line Resource (Beijing, China). E.G7-OVA cell line was purchased from Bioleaf (Shanghai, China).

4.2. Agarose gel retention assay

OVA (8 μ g) were respectively mixed with DA1, DA2, DA3, DA4, DA5 and DA6 at a certain mass ratio of 1:4. Then crosslinking agents C1-C3 were respectively added to the mixture at a certain molar ratios. For C1 and C2, the molar ratio of C1 or C2 to DA1–6 was 1:3, for C3, the molar ratio of C3 to DA1–6 was 1:4. All samples were subjected to 1 h electrophoresis on 1% agarose gel and then the images were collected by gel imaging instrument (Gel Doc Bio-Rad).

4.3. Uptake of OVA-FITC by RAW264.7 cells

Cellular uptake studies were performed in RAW264.7 cells at an initial cell density of 1×10^4 in 96-well plate. After overnight incubation, cells were treated with various OVA-FITC nanoformulations and incubated for another 8 h. The cells were then slowly washed with PBS and stained with DAPI after fixing with paraformaldehyde. Cell images were acquired by fluorescence microscopy (Olympus IX 51). After that, the cells were trypsinized, centrifuged and resuspended in PBS for flow

cytometry analysis.

4.4. Cytokine release in RAW264.7

RAW264.7 cells were seeded in 24 well plates with a cell density of 4×10^4 cells per well. After overnight incubation, the cells were washed with PBS and treated with different nanoformulations including OVA+CpG, DA2C3/OVA, DA2C3/OVA/CpG, DA4C3/OVA/CpG, DA5C1/OVA, DA5C1/OVA/CpG, DA6C1/OVA, DA6C1/OVA/CpG with equal concentration of OVA (10 $\mu\text{g}/\text{mL}$) and CpG (0.4 $\mu\text{g}/\text{mL}$). After incubating for another 8 h, the media were collected and centrifuged at 12000 rpm for 15 min at 4 °C. The levels of TNF- α were determined by enzyme-linked immune sorbent assay (ELISA) according to the instructions.

4.5. Bone marrow-derived dendritic cells

Bone marrow-derived DCs (BMDCs) were collected from the bone marrow of C57BL/6 mice. Briefly, after repeated washing of mouse bone marrow, the cell suspension passed through a 200 mesh cell sieve. Then red blood cell (RBC) lysate was added to remove red blood cells. The RBC depleted bone marrow cells (3×10^6 cells/mL) were plated in a 12 well plate in complete 1640 medium supplemented with GM-CSF (20 ng/mL) and interleukin-4 (10 ng/mL) at 37 °C and 5% CO₂. The culture medium was removed and replenished every three days, and the cells could be used for relative experiments after one week of culture.

4.6. Cellular uptake and cytotoxicity studies

In the cell uptake study, free OVA+CpG and DA6C1/OVA-FITC/CpG-ROD were incubated with immature BMDCs respectively. After overnight incubation, DAPI was used to locate the nuclei. The cells were then imaged by confocal microscopy (Becton Dickinson, San Jose, CA) and analyzed by flow cytometry after digestion. The cell cytotoxicity was determined by the cell counting kit-8 (CCK-8) assay following the standard protocol.

4.7. In vitro BMDCs activation, antigen cross-presentation and cytokine release analysis

Immature BMDCs cells (3×10^6 cells/mL) were implanted in a 12 well plate for 12 h and then treated with OVA+CpG, DA6C1/OVA and DA6C1/OVA/CpG with equal concentration of OVA (10 $\mu\text{g}/\text{mL}$) and CpG (0.4 $\mu\text{g}/\text{mL}$). After 24 h of incubation, the supernatants of BMDCs were measured by ELISA to determine the release of TNF- α and IL-6 following the instructions. Flow cytometry analysis was performed to analyze the percentage of antigen cross-presentation and activation of DCs. Cells and suspended in PBS were incubated with Cy5.5-anti mouse CD11c, APC-anti SIINFEKL / H-2Kb for 30 min at low temperature for antigen cross-presentation assay or with Cy5.5-anti mouse CD11c, APC-anti mouse CD80 and FITC-anti mouse CD86 for DC maturation analysis.

4.8. Animal model

All animal experiments were carried out in compliance with the requirements of the National Act on the Use of Experimental Animals (People's Republic of China) and were approved by the Experimental Animal Ethical Committee of Chongqing University Cancer Hospital. Female C57BL/6 mice (16–20 g) were supplied by the Animal Center of Chongqing Medical University (Chongqing, China).

4.9. In vivo tracking of various labeled vaccine formulations

To observe antigen persistence at the site of vaccination and migration to the draining lymph nodes, OVA were labeled by Rhodamine (ROD). Various labeled vaccine formulations including OVA-ROD/

CpG or DA6C1/OVA-ROD/CpG were injected subcutaneously into the tail base of C57BL/6 mice. Small animal imaging system (IVIS Lumina III) was utilized to observe in situ ROD fluorescence at the injection site and draining inguinal lymph nodes at different time points. 24 h post injection, major organs including heart, liver, spleen, lung, kidney and inguinal lymph nodes were excised from euthanized mice for ex vivo ROD fluorescent imaging.

4.10. Prophylactic vaccination and tumor challenge

C57BL/6 mice were subcutaneously inoculated with different vaccine formulations including OVA+CPG, DA6C1/OVA or DA6C1/OVA/CpG with equal amount of OVA (2.5 mg/kg) and CpG (100 $\mu\text{g}/\text{kg}$) every seven days for a total of three times. PBS was used as the control group. At day 21, the immunized mice were injected subcutaneously with E.G7-OVA cells (5×10^5). The tumor sizes and survival rate of the mice were measured every other day during the experiment. The tumor volume was calculated by using the following equation: tumor volume V (mm^3) = L x W x W/2 (L: tumor length, W: tumor width).

4.11. Therapeutic effect in combination with anti-PD1

C57BL/6 mice were injected subcutaneously with E.G7-OVA cells (5×10^5). On the fifth day after tumor cell inoculation, mice were subcutaneously inoculated with different vaccine formulations including OVA+CPG, DA6C1/OVA or DA6C1/OVA/CpG with equal amount of OVA (2.5 mg/kg) and CpG (100 $\mu\text{g}/\text{kg}$) every six days for a total of three times. Alternatively, mice from some groups were intraperitoneally injected with anti-PD1 at the dose of 150 μg per mouse on day 5, 8, 11, 14 and 17 for comparison or combination therapy. PBS was used as the control group. The tumor sizes and survival rate of the mice were measured every other day. Mice were euthanized when the tumor volumes reached 3000 mm^3 . On the 21st day, the tumor of each group of mice was separated and collected. After the cell suspension was prepared by mechanical grinding, fluorescent antibodies were added as follows. For labeling T Cells, FITC-anti mouse CD3, APC-anti mouse CD4 and PE-anti mouse CD8 were added. For labeling Tregs, FITC-anti mouse CD3, APC-anti mouse CD4 and PE-anti mouse Foxp3 were added. Both of them were incubated at 4 °C for half an hour. The percentage of T cells and Tregs in tumor tissue was determined by flow cytometry. In order to study the distribution of CD8⁺ T cells (CTLs) and IFN- γ in tumor tissues, frozen sections of tumor tissues were incubated with DAPI, anti-CD8-PE, or anti-IFN- γ -FITC respectively, and then observed by confocal microscopy. To further evaluate the therapeutic effect, section of tumor was stained with H&E for histology analysis. In addition, tissues section, heart, liver, spleen, lung and kidney were stained with H&E for histological analysis to evaluate the safety of nanovaccine.

4.12. Lymph node analysis

The inguinal lymph nodes were removed from mice vaccinated with different samples including OVA+CPG, DA6C1/OVA or DA6C1/OVA/CpG, and PBS was used as the control group. Cell suspensions from the lymph nodes were then stained with Cy5.5-anti mouse CD11c, FITC-anti mouse CD86 and APC-anti mouse CD80 antibodies for 30 min at 4 °C to evaluate the DC maturation. For analysis of DC cross-presentation, the single cell suspensions were stained with FITC-anti mouse CD11c and PE-anti mouse SIINFEKL/H-2Kb (MHC I) at 4 °C for 30 min and analyzed by flow cytometry.

4.13. Serum levels of cytokine

Mice were inoculated with different formulations including OVA+CPG, DA6C1/OVA, DA6C1/OVA/CpG with equal amount of OVA (2.5 mg/kg) and CpG (100 $\mu\text{g}/\text{kg}$) every seven days for a total of three times. PBS was used as the control group. On the 21st day after

inoculation, sera were collected and then measured with ELISA kits to determine the levels of TNF- α , IFN- γ and IL-6.

4.14. Titer measurement

Serum samples were collected 7 days after the third immunization of mice with OVA+CpG, DA6C1/OVA or DA6C1/OVA/CpG. Micro titer plate (96-well, Costar) was coated with OVA (10 $\mu\text{g}/\text{mL}$) in PBS (100 μL) at 4 $^{\circ}\text{C}$ for 24 h. The wells were then washed twice with PBST (PBS containing 0.01% Tween 20) and incubated with blocking buffer (5% BSA in PBST) at 37 $^{\circ}\text{C}$ for 1 h. After being washed three times, 100 μL serially diluted mouse serum (1:1000) were added to each well and incubated at 37 $^{\circ}\text{C}$ for another 4 h. The wells were then washed three times with PBST and incubated with 100 μL horseradish peroxidase-conjugated goat anti-mouse IgG (diluted 1:20000 in ELISA diluted buffer). After being incubated at 37 $^{\circ}\text{C}$ for 2 h, the wells were then extensively washed and added with TMB solution. After incubation for 30 min at room temperature, 50 μL H_2SO_4 (2 M) was added to each well to stop color development and the absorbance was measured at 490 nm to evaluate the production of anti-OVA IgG titers.

4.15. Splenocytes proliferation assay

Mice were inoculated with different formulations including OVA+CPG, DA6C1/OVA or DA6C1/OVA/CpG with equal amount of OVA (2.5 mg/kg) and CpG (100 $\mu\text{g}/\text{kg}$) every seven days for a total of three times. PBS was used as the control group. Mice were sacrificed on day 21 and splenocytes were isolated and seeded into 96-well plate. After 8 h incubation at 37 $^{\circ}\text{C}$ in a humid atmosphere with 5% CO_2 , the cells were treated with OVA (50 $\mu\text{g}/\text{mL}$) and incubated for another 72 h. The proliferation of splenocytes was then evaluated by CCK-8 assay.

4.16. Activation of cytotoxic T-lymphocytes

According to the above described method, the splenocytes were extracted from the spleen of immunized mice 7 d after the third immunization and seeded in a 24 well plate. Cells were restimulated with OVA (50 $\mu\text{g}/\text{mL}$) for 72 h and then stained with FITC-anti mouse CD3, APC-anti mouse CD4 or PE-anti mouse CD8 for FACS analysis. Supernatant of splenocytes treated with different vaccine formulations were collected and detected IFN- γ by ELISA Kit.

4.17. Statistics

All results were expressed as mean values \pm Standard deviation, as shown in figures. The student's *t*-test was used to compare the two groups. All experimental data was analyzed by Prism software package (prism 8.0; Graphpad software). The statistical significance threshold was $P < 0.05$.

Data availability

All data are either provided in the figures, supplementals or are otherwise available upon request.

Declaration of Competing Interest

The authors declare that they have no known competing financial interests or personal relationships that could have appeared to influence the work reported in this paper.

Acknowledgements

This work was supported by National Natural Science Foundation of China (21773268, 21877010), Fundamental Research Funds for the Central Universities (2019CDYGYB006), Chongqing Graduate Student

Research Innovation Project (CYB18056, CYB19067), and the Startup Funding of Chongqing University (0236011104419).

Appendix A. Supplementary data

Supplementary data to this article can be found online at <https://doi.org/10.1016/j.jconrel.2021.07.033>.

References

- [1] H. Dewitte, R. Verbeke, K. Breckpot, S.C. De Smedt, I. Lentacker, Nanoparticle design to induce tumor immunity and challenge the suppressive tumor microenvironment, *Nano Today* 9 (2014) 743–758.
- [2] W. Deng, W.J. Chen, S. Clement, A. Guller, Z.J. Zhao, A. Engel, E.M. Goldys, Controlled gene and drug release from a liposomal delivery platform triggered by X-ray radiation, *Nat. Commun.* 9 (2018) 2713.
- [3] C. Iclozan, S. Antonia, A. Chiappori, D.T. Chen, D. Gabrilovich, Therapeutic regulation of myeloid-derived suppressor cells and immune response to cancer vaccine in patients with extensive stage small cell lung cancer, *Cancer Immunol. Immun.* 62 (2013) 909–918.
- [4] M.M. Gubin, X.L. Zhang, H. Schuster, E. Caron, J.P. Ward, T. Noguchi, Y. Ivanova, J. Hundal, C.D. Arthur, W.J. Krebber, G.E. Mulder, M. Toebes, M.D. Vesely, S.S. K. Lam, A.J. Korman, J.P. Allison, G.J. Freeman, A.H. Sharpe, E.L. Pearce, T. N. Schumacher, R. Aebbersold, H.G. Rammensee, C.J.M. Melief, E.R. Mardis, W. E. Gillanders, M.N. Artyomov, R.D. Schreiber, Checkpoint blockade cancer immunotherapy targets tumour-specific mutant antigens, *Nature* 515 (2014) 577–581.
- [5] J.M. Kirkwood, L.H. Butterfield, A.A. Tarhini, H. Zarour, P. Kalinski, S. Ferrone, Immunotherapy of cancer in 2012, *Ca-Cancer J. Clin.* 62 (2012) 309–335.
- [6] D. Fukumura, J. Kloepper, Z. Amoozgar, D.G. Duda, R.K. Jain, Enhancing cancer immunotherapy using antiangiogenics: opportunities and challenges, *Nat. Rev. Clin. Oncol.* 15 (2018) 325–340.
- [7] Y. Zhang, F.M. Wang, E.G. Ju, Z. Liu, Z.W. Chen, J.S. Ren, X.G. Qu, Metal-organic-framework-based vaccine platforms for enhanced systemic immune and memory response, *Adv. Funct. Mater.* 26 (2016) 6454–6461.
- [8] L.H. Zhang, S.J. Wu, Y. Qin, F. Fan, Z.M. Zhang, C.L. Huang, W.H. Ji, L. Lu, C. Wang, H.F. Sung, X.G. Leng, D.L. Kong, D.W. Zhu, Targeted Codelivery of an antigen and dual agonists by hybrid nanoparticles for enhanced Cancer immunotherapy, *Nano Lett.* 19 (2019) 4237–4249.
- [9] W.J. Shan, H.P. Zheng, G.F. Fu, C.F. Liu, Z.Z. Li, Y.H. Ye, J. Zhao, D. Xu, L.P. Sun, X. Wang, X.L. Chen, S.L. Bi, L. Ren, G. Fu, Bioengineered nanocage from Hbc protein for combination cancer immunotherapy, *Nano Lett.* 19 (2019) 1719–1727.
- [10] K.Y. Ni, T.K. Luo, G.X. Lan, A. Culbert, Y. Song, T. Wu, X.M. Jiang, W.B. Lin, A nanoscale metal-organic framework to mediate photodynamic therapy and deliver CpG oligodeoxynucleotides to enhance antigen presentation and cancer immunotherapy, *Angew. Chem. Int. Edit.* 59 (2020) 1108–1112.
- [11] Y. Tao, E.G. Ju, Z.H. Li, J.S. Ren, X.G. Qu, Engineered CpG-antigen conjugates protected gold nanoclusters as smart self-vaccines for enhanced immune response and cell imaging, *Adv. Funct. Mater.* 24 (2014) 1004–1010.
- [12] D.W. Zhu, C.Y. Hu, F. Fan, Y. Qin, C.L. Huang, Z.M. Zhang, L. Lu, H. Wang, H. F. Sun, X.G. Leng, C. Wang, D.L. Kong, L.H. Zhang, Co-delivery of antigen and dual agonists by programmed mannose-targeted cationic lipid-hybrid polymersomes for enhanced vaccination, *Biomaterials* 206 (2019) 25–40.
- [13] J.T. Wilson, S. Keller, M.J. Manganiello, C. Cheng, C.C. Lee, C. Opara, A. Convertine, P.S. Stayton, pH-responsive nanoparticle vaccines for dual-delivery of antigens and immunostimulatory oligonucleotides, *ACS Nano* 7 (2013) 3912–3925.
- [14] Q. Chen, M.C. Chen, Z. Liu, Local biomaterials-assisted cancer immunotherapy to trigger systemic antitumor responses, *Chem. Soc. Rev.* 48 (2019) 5506–5526.
- [15] S.Q. Yan, Z.C. Luo, Z.L. Li, Y. Wang, J. Tao, C.Y. Gong, X.G. Liu, Inside cover: synergistic n-heterocyclic carbene/palladium-catalyzed umpolung 1,4-addition of aryl iodides to enals, *Angew. Chem. Int. Edit.* 59 (2020) 2–14.
- [16] X.P. Wang, S. Ihara, X. Li, A. Ito, Y. Sogo, Y. Watanabe, A. Yamazaki, N.M. Tsuji, T. Ohno, Rod-scale design strategies for immune-targeted delivery system toward cancer immunotherapy, *ACS Nano* 13 (2019) 7705–7715.
- [17] C. Wang, Y.Q. Ye, Q.Y. Hu, A. Bellotti, Z. Gu, Tailoring biomaterials for cancer immunotherapy: emerging trends and future outlook, *Adv. Mater.* 29 (2017) 1606036.
- [18] H. Zhao, J. Xu, Y. Li, X.X. Guan, X. Han, Y.Y. Xu, H.T. Zhou, R. Peng, J. Wang, Z. Liu, Nanoscale coordination polymer based nanovaccine for tumor immunotherapy, *ACS Nano* 13 (2019) 13127–13135.
- [19] W.T. Song, S.N. Musetti, L. Huang, Nanomaterials for cancer immunotherapy, *Biomaterials* 148 (2017) 16–30.
- [20] D.S. Wilson, S. Hirose, M.M. Raczky, L. Bonilla-Ramirez, L. Jeanbart, R.Y. Wang, M. Kwissa, J.F. Franetich, M.A.S. Broggi, G. Diaceri, X. Quaglia-Thermes, D. Mazier, M.A. Swartz, J.A. Hubbell, Antigens reversibly conjugated to a polymeric glyco-adjuvant induce protective humoral and cellular immunity, *Nat. Mater.* 18 (2019) 175–185.
- [21] C. Xu, J. Nam, H. Hong, Y. Xu, J.J. Moon, Positron emission tomography-guided photodynamic therapy with biodegradable mesoporous silica nanoparticles for personalized cancer immunotherapy, *ACS Nano* 13 (2019) 12148–12161.
- [22] H.A.F.M. Hassan, L. Smyth, J.T.W. Wang, P.M. Costa, K. Ratnasothy, S.S. Diebold, G. Lombardi, K.T. Al-Jamal, Dual stimulation of antigen presenting cells using

- carbon nanotube-based vaccine delivery system for cancer immunotherapy, *Biomaterials* 104 (2016) 310–322.
- [23] X.P. Duan, C. Chan, W.B. Lin, Nanoparticle-mediated immunogenic cell death enables and potentiates cancer immunotherapy, *Angew. Chem. Int. Edit.* 58 (2019) 670–680.
- [24] X.D. Qi, X.W. Liu, L. Matiski, R.R. Del Villar, T. Yip, F. Zhang, S. Sokalingam, S. X. Jiang, L. Liu, H. Yan, Y. Chang, RNA origami nanostructures for potent and safe anticancer immunotherapy, *ACS Nano* 14 (2020) 4727–4740.
- [25] W.T. Song, K. Tiruthani, Y. Wang, L.M. Shen, M.Y. Hu, O. Dorosheva, K.Y. Qiu, K. A. Kinghorn, R.H. Liu, L. Huang, Trapping of lipopolysaccharide to promote immunotherapy against colorectal cancer and attenuate liver metastasis, *Adv. Mater.* 30 (2018) 1805007.
- [26] N.O. Fischer, A. Rasley, C. Blanchette, Nanoparticles and antigen delivery: understanding the benefits and drawbacks of different delivery platforms, *Nanomedicine-Uk* 9 (2014) 373–376.
- [27] P. Zhang, X.G. Liu, P. Liu, F. Wang, H. Ariyama, T. Ando, J.P. Lin, L.H. Wang, J. Hu, B. Li, C.H. Fan, U1 snRNP regulates cancer cell migration and invasion in vitro, *Nat. Commun.* 11 (2020) 1–9.
- [28] R.S. Riley, C.H. June, R. Langer, M.J. Mitchell, Delivery technologies for cancer immunotherapy, *Nat. Rev. Drug Discov.* 18 (2019) 175–196.
- [29] J.M. Caster, C. Callaghan, S.N. Seyedin, K. Henderson, B. Sun, A.Z. Wang, Optimizing advances in nanoparticle delivery for Cancer immunotherapy, *Adv. Drug Deliv. Rev.* 144 (2019) 3–15.
- [30] M.R. Jones, N.C. Seeman, C.A. Mirkin, Programmable materials and the nature of the DNA bond, *Science* 347 (2015) 1260901.
- [31] T. Aida, E.W. Meijer, S.I. Stupp, Functional supramolecular polymers, *Science* 335 (2012) 813–817.
- [32] M.J. Webber, E.A. Appel, E.W. Meijer, R. Langer, Supramolecular biomaterials, *Nat. Mater.* 15 (2016) 13–26.
- [33] M. Delfi, R. Sartorius, M. Ashrafzadeh, E. Sharifi, Y.P. Zhang, P.D. Berardinis, A. Zarrabi, R.S. Varma, F.R. Tay, B.R. Smith, P. Makvandi, Self-assembled peptide and protein nanostructures for anti-cancer therapy: Targeted delivery, stimuli-responsive devices and immunotherapy, *Nano Today* 38 (2021) 101119.
- [34] E.N. Zara, X.Q. Zheng, P. Makvandi, H. Gheybi, R. Sartorius, C.K.Y. Yiu, M. Adeli, A.M. Wu, A. Zarrabi, R.S. Varma, F.R. Tay, Nonspherical metal-based nanoarchitectures: synthesis and impact of size, shape, and composition on their biological activity, *Small* 17 (2021) 2007073.
- [35] A.R. Thomson, C.W. Wood, A.J. Burton, G.J. Bartlett, R.B. Sessions, R.L. Brady, D. N. Woolfson, Computational design of water-soluble α -helical barrels, *Science* 346 (2014) 485–488.
- [36] K.E. Inostroza-Brito, E. Collin, O. Siton-Mendelson, K.H. Smith, A. Monge-Marcet, D.S. Ferreira, R.P. Rodriguez, M. Alonso, J.C. Rodriguez-Cabello, R.L. Reis, F. Sagues, L. Botto, R. Bitton, H.S. Azevedo, A. Mata, Co-assembly, spatiotemporal control and morphogenesis of a hybrid protein-peptide system, *Nat. Chem.* 7 (2015) 897–904.
- [37] C.G. Pappas, R. Shafi, I.R. Sasselli, H. Siccardi, T. Wang, V. Narang, R. Abzalimov, N. Wijerathne, R.V. Ulijn, Dynamic peptide libraries for the discovery of supramolecular nanomaterials, *Nat. Nanotechnol.* 11 (2016) 960–967.
- [38] X.B. Zhao, F. Pan, H. Xu, M. Yaseen, H.H. Shan, C.A.E. Hauser, S.G. Zhang, J.R. Lu, Molecular self-assembly and applications of designer peptide amphiphiles, *Chem. Soc. Rev.* 39 (2010) 3480–3498.
- [39] M. Kumar, N.L. Ing, V. Narang, N.K. Wijerathne, A.I. Hochbaum, R.V. Ulijn, Amino-acid-encoded biocatalytic self-assembly enables the formation of transient conducting nanostructures, *Nat. Chem.* 10 (2018) 696–703.
- [40] Y. Engelberg, M. Landau, The human LL-37(17–29) antimicrobial peptide reveals a functional supramolecular structure, *Nat. Commun.* 11 (2020) 3894.
- [41] R. Mohammadinejad, A. Dehshahri, V.S. Madamsetty, M. Zahmatkeshan, S. Tavakol, P. Makvandi, D. Khorsandi, A. Pardakhty, M. Ashrafzadeh, E.G. Afshar, A. Zarrabi, In vivo gene delivery mediated by non-viral vectors for cancer therapy, *J. Control. Release* 325 (2020) 249–275.
- [42] Z.C. Luo, Q.J. Wu, C.B. Yang, H.M. Wang, T. He, Y.Z. Wang, Z.Y. Wang, H. Chen, X. Y. Li, C.Y. Gong, Z.M. Yang, A powerful CD8⁺ T-cell stimulating d-tetra-peptide hydrogel as a very promising vaccine adjuvant, *Adv. Mater.* 29 (2017) 1601776.
- [43] J. Song, C. Yuan, T. Jiao, R. Xing, M. Yang, D.J. Adams, X. Yan, Multifunctional antimicrobial biometallohydrogels based on amino acid coordinated self-assembly, *Small* 16 (2020), e1907309.
- [44] N. Kim, W. Kim, S.Y. Lee, J.E. Yin, Y. Lee, J.H. Lim, S.Y. Kim, E.S. Duong, H. Thuy, T.H. Kim, K. Kim, S. Kim, J.E. Lee, D.S. Kim, J. Lee, M.S. Lim, Y.T. Jeong, J. H. enhanced Cancer vaccination by in situ Nanomicelle-generating dissolving microneedles, *ACS Nano* 12 (2018) 9702–9713.
- [45] K. Liu, R.R. Xing, Q.L. Zou, G.H. Ma, H. Mçhwald, X.H. Yan, Simple peptide-tuned self-assembly of photosensitizers towards anticancer photodynamic therapy, *Angew. Chem. Int. Edit.* 55 (2016) 3036–3039.
- [46] H. Zhang, K. Liu, S.K. Li, X. Xin, S.L. Yuan, G.H. Ma, X.H. Yan, Self-assembled minimalist multifunctional Theranostic Nanoplatform for magnetic resonance imaging-guided tumor photodynamic therapy, *ACS Nano* 12 (2018) 8266–8276.
- [47] S. Bera, B. Xue, P. Rehak, G. Jacoby, W. Ji, L.J.W. Shimon, R. Beck, P. Král, Y. Cao, E. Gazit, Self-assembly of aromatic amino acid enantiomers into supramolecular materials of high rigidity, *ACS Nano* 14 (2020) 1694–1706.